Rapid Communications

Simulating the spectral gap with polariton graphs

Kirill P. Kalinin,[1] Sergey Alyatkin,[2] Pavlos G. Lagoudakis,[2,3] Alexis Askitopoulos,[2] and Natalia G. Berloff[2,1,*]

[1]*Department of Applied Mathematics and Theoretical Physics, University of Cambridge, Cambridge CB3 0WA, United Kingdom*

[2]*Skolkovo Institute of Science and Technology, Nobelya Ulitsa 3, Moscow 121205, Russian Federation*

[3]*Department of Physics and Astronomy, University of Southampton, Southampton SO17 1BJ, United Kingdom*

(Received 28 October 2020; accepted 30 October 2020; published 20 November 2020)

Polariton graphs were recently proposed and validated as a novel platform for solving hard optimization problems that can be mapped into the Ising or XY models. Here, we elucidate a relationship between the energy spectrum of the XY Hamiltonian, Hermitian and non-Hermitian, and the total number of condensed polariton particles. Using a hexagonal unit lattice we show that the lower-energy states of the XY Hamiltonian are faithfully reproduced by mean-field simulations. We further confirm experimentally a possibility of finite spectral gaps near the condensation threshold for the triangular lattice configurations of polariton condensates. Our study paves the way to simulating the spectral gap of Hermitian and non-Hermitian XY models using polariton graphs.

DOI: 10.1103/PhysRevB.102.180303

It is hard to identify a physical concept as important in condensed matter physics as the notion of the spectral gap. Often physical behaviors can be understood through analysis of energy spectra and the difference between the two lowest-energy levels, known as the spectral gap, determines the phase diagram of physical systems. When the spectral gap vanishes, phase transitions occur. Whereas critical behavior is associated with gapless systems, wherein long-range correlations are supported by low-energy excitations that behave as massless particles, noncritical behavior is associated with gapped systems, wherein long-range correlations are prevented through massive low-energy excitations [1]. In adiabatic quantum computation that can be as powerful as the usual circuit model for quantum computation [2], the spectral gap is a crucial quantity that defines the efficiency of a quantum algorithm. Such an algorithm is efficient only if there exists a Hamiltonian path for which the minimal spectral gap is lower bounded by an inverse polynomial in the system size [3]. Finding a method that allows one to determine whether or not a quantum many-body Hamiltonian is gapped, or even calculate the size of the gap, is one of the fundamental questions for condensed matter systems. Even for some simple spin models on one- and two-dimensional (1D and 2D) lattices, there are famous outstanding problems on the existence of the spectral gap [4,5]. Recently, the undecidability of the spectral gap problem was rigorously proven, meaning that it is algorithmically impossible to say whether a general Hamiltonian is gapped or gapless [6]. Hence, one cannot extrapolate the discovered patterns in large, but still computable systems, to larger systems that are incomputable. An alternative way to determine if a given large system, for which the spectral gap cannot be calculated using the classical Turing algorithm and classical hardware, is to use unconventional computing systems. Such systems have been explored with proposals ranging from the universal quantum computations and quantum simulators (for a review, see Ref. [7]) to, more recently, analog Hamiltonian simulators [8–13].

Various physical systems have been proposed and realized to a various degree of scalability and efficiency. Ultracold atoms in optical lattices [14–17], trapped ions [18,19], photons [20], superconducting qubits [21], network of optical parametric oscillators (OPOs) [8,9], coupled lasers [11], multimode cavity QED [12], and photon condensates [13] are among the most promising systems proposed to overcome the limitations of the classical Turing computation. The existence of universal spin Hamiltonians, such as the two-dimensional Ising model on a square lattice with next-neighbor interactions and fields [22], implies that the successful emulation of certain simple Hamiltonians on unconventional computing platforms could be generalized to simulations of any other classical spin model with arbitrary long-range many-body interactions.

Another novel platform for simulating spin Hamiltonians is based on polariton networks [10]. Polaritons are the composed light-matter bosonic quasiparticles formed in the strong exciton-photon coupling regime in semiconductor microcavities [23]. Due to bosonic stimulation polaritons condense in the same quantum mechanical state [24–26]. Using spatial modulation and nonresonant optical excitation, polaritons can be made to condense at any location of a planar microcavity forming a two-dimensional graph of condensates [27]. When the coherence lifetime of polaritons exceeds the time of flight between neighboring sites (graph vertices), polariton interactions lead to the development of phase relationships across the vertices [28–30]. As polaritons condense to the same quantum mechanical state, the phases of polaritons at the pumping sites become either locked with particular phase differences or oscillate between unstable fixed points. Such phase difference behavior represents many oscillator models [31] including Kuramoto, Stuart-Landau, Lang-Kobayashi, and others depending on the system parameters: lattice and pump geometry and microcavity structure. For a certain range of parameters, the phase configurations of polariton networks may

*Author to whom correspondence should be addressed: N.G.Berloff@damtp.cam.ac.uk

correspond to the ground state of the XY Hamiltonian. The connection between the minimization of the XY Hamiltonian and the maximization of the number particles at the condensation threshold was first established for simple geometrically coupled polariton graphs [10] and further generalized to simulations of discrete and continuous spins Hamiltonians with polariton pillars and remote couplings [32,33]. The process of identifying the ground state of the XY Hamiltonian through bosonic stimulation is very similar to that of coupled lasers [11,34].

In this Rapid Communication, we establish that polariton graphs are not only capable of finding the ground state of the XY model, but also the low-energy spectrum of the excited states, and therefore can become an efficient tool for retrieving the spectral gap of various oscillator models and the XY Hamiltonians. The energy landscape of the XY Hamiltonian is set by the interaction strengths J_{ij} that depend on the pumping intensity and the graph geometry. We show that higher-energy levels of the XY Hamiltonian have a progressively lower occupancy while showing up on the energy spectrum of polaritonic systems both above or below the state that corresponds to the ground state of the XY Hamiltonian. We shall refer to the state with the second largest particle number as "the first excited state," where the difference in the number of particles between the ground and first excited state represents the spectral gap of the XY model. If the system parameters are such that interaction couplings of the XY Hamiltonian are complex, which happens when a Josephson type of coupling is combined with a dissipative one [31], the XY Hamiltonian is non-Hermitian. Studies of non-Hermitian XY models were addressed using three-level atoms in a variety of setups, including trapped ions, cavity QED, and atoms in optical lattices [35]. Such systems attracted attention as they provide the opportunity to discover new classes of phase transitions beyond the framework of Hermitian critical phenomena. In this case, the energy gap provides the information about the exceptional and bifurcation points of a non-Hermitian Hamiltonian [31,36]. Such points manifest themselves through the emergence of sidebands and intensity peaks [37]; their position is important, for instance, in heteroclinic computing [38–40].

The XY model on different types of lattices, such as triangular [41], square [42–44], and honeycomb [45–47], is usually considered in terms of the frustration parameter J_2/J_1 representing the ratio of the strength of the next-neighbor interactions J_2 to the nearest-neighbor interaction J_1. A system may exhibit different phase configurations depending on this value: collinear ordering (i.e., antiferromagnetic ordering, Néel state I, classical order), the state of a quantum spin liquid (i.e., Bose metal), collinear ordering when two of the three nearest-neighboring spins are antiparallel, and the other are parallel (i.e., Néel state II, anti-Néel, collinear spin wave). The XY model on a honeycomb lattice has attracted much attention of experimental and theoretical physicists, since a small number of neighbor interactions enhances quantum fluctuations, and therefore it seems to be a promising system for obtaining spin-liquid states. It was initially believed [45] that for a simple XY spin model, a specific spin-liquid ground state, a Bose liquid, appears for a particular range of the frustration parameter, while a surprising antiferromagnetic Ising phase was detected [46] for the same range by examining

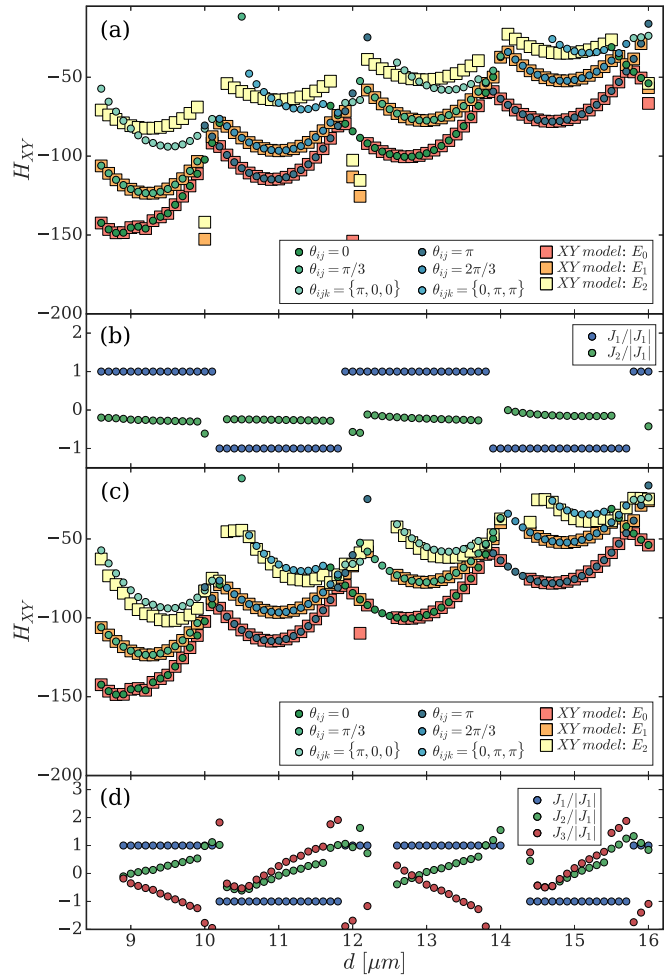

FIG. 1. (a), (c) The three lowest-energy levels of the XY model (squares) and the particle mass residues of polariton condensates (circles) as functions of the hexagon side d. The particle mass residues are calculated by numerical integration of Eqs. (3) and (4) as described in the main text. The color of the circles represents different phase configurations with the description given in the legend. The first three energy levels for the (a) J_1-J_2 model and (c) J_1-J_2-J_3 model are found by the direct minimization of the XY Hamiltonian using the gain-dissipative algorithm and shown with red, orange, and yellow squares. Their phase configurations are similar to the phases shown with circles over which the squares are plotted. The coupling ratios with respect to the hexagon side d found from Eqs. (3) and (4), as described in the text, are plotted for the (b) J_1-J_2 model and (d) J_1-J_2-J_3 model.

much larger lattices without finding any spin-liquid ground state. By considering models with second-neighbor J_1-J_2 or even third-neighbor J_1-J_2-J_3 interactions, possible symmetry-breaking ground states were shown on a honeycomb lattice [47,48].

The total number of condensed polaritons in the system with l equally pumped spots can be expressed as [10]

$$N = \int |\psi(\mathbf{r},t)|^2 d\mathbf{r} \approx lN_0 + \sum_{i<j} J_{ij}(k_c, d_{ij}) \cos\theta_{ij}, \quad (1)$$

where $\psi(\mathbf{r},t)$ is the condensate wave function, and N_0 represents the number of polaritons of one isolated pumping

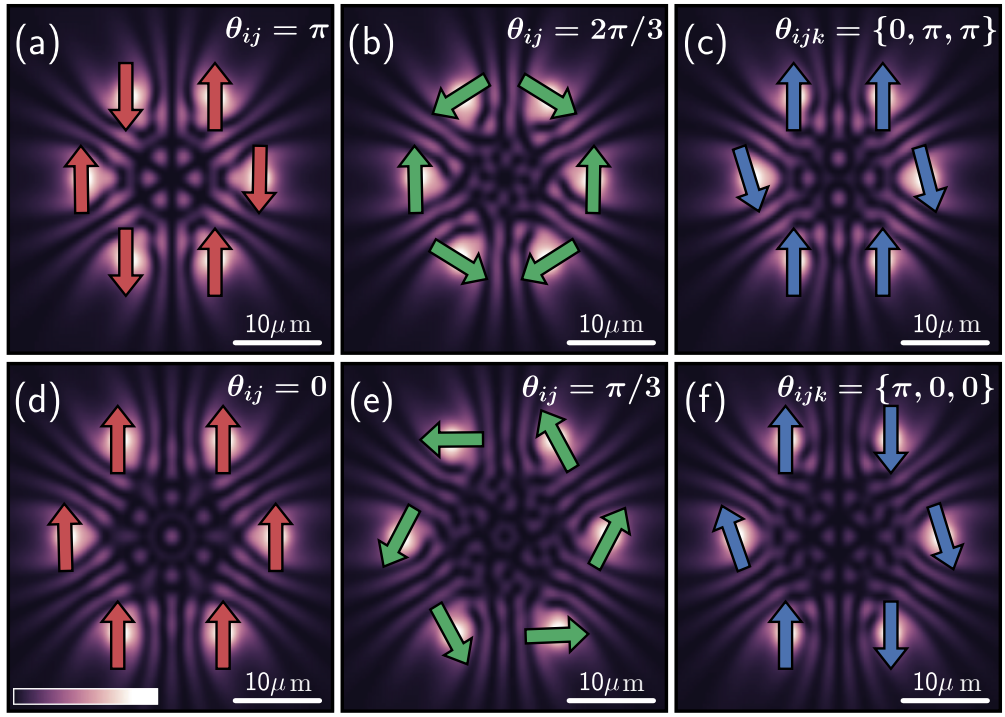

FIG. 2. The polariton densites for the hexagons with the sides (a)–(c) $d = 11$ μm and (d)–(f) $d = 13$ μm found by numerical integration of Eqs. (3) and (4). The first row shows (a) an AF ordering for the ground state (Néel's ordering), (b) a double vortex, and (c) a spin wave for the two lowest excited states (Néel state II). The second row depicts (d) a F ordering, (e) a single vortex state, and (f) a different spin-wave state (Néel state III). The arrows correspond to the phases of the condensates. The indices j and k stand here for the short notation of $i + 1$ and $i + 2$ neighbor condensates, respectively.

spot. J_{ij} stands for the interaction strength between polariton spots at positions $\mathbf{r} = \mathbf{r}_i$ and $\mathbf{r} = \mathbf{r}_j$, separated by the distance $d_{ij} = |\mathbf{r}_i - \mathbf{r}_j|$ with outflow velocities k_c. Here, $\theta_{ij} = \theta_i - \theta_j$ is the relative phase difference between the polaritons at $\mathbf{r}_i$ and $\mathbf{r}_j$. From Eq. (1) we can define the *particle mass residue* $\mathcal{M} = lN_0 - N$ that represents the change in the number of particles in the system due to the interaction of the condensates among different pumping spots. The expression for $\mathcal{M}$ from Eq. (1) approximates the definition of the XY Hamiltonian, $H_{XY} = -\sum_{i<j} J_{ij} \cos\theta_{ij}$. The particle mass residue of polariton states corresponds to the energy spectra of the XY model, while the particle mass residue difference between the ground and first excited state approximates its spectral gap.

We elucidate this argument by considering a hexagon unit cell with size $d = |\mathbf{r}_i - \mathbf{r}_{i+1}|$ and the pumping profile $P = \sum_{i=1}^{6} P_0 \exp(-\alpha|\mathbf{r} - \mathbf{r}_i|^2)$, where α is the inverse width of the Gaussian. The particle mass residue becomes $\mathcal{M} = 6N_0 - N_{\text{hex}}$, where N_{hex} is the number of particles in the hexagon of polariton condensates and the XY Hamiltonian becomes

$$H_{XY} = -J_1 \sum_{i=1}^{6} \cos\theta_{ii+1} - J_2 \sum_{i=1}^{6} \cos\theta_{ii+2} - J_3 \sum_{i=1}^{3} \cos\theta_{ii+3}, \tag{2}$$

where the summation is cyclic in i (e.g., $i + 1$ is set to 1 for $i = 6$) and where we included all pairwise interactions between vertices. Experimentally, the number of particles in the system and therefore the particle mass residues of the ground and then the lower excited states are determined as the pumping intensity P_0 approaches the condensation threshold from below and then exceeds it. This constitutes the speedup in comparison with the classical computer minimization that requires an extensive search of the minima of an energy configuration of a high dimensionality fixed by the lattice size. For only six pumping spots we can compute the particle mass residues for the lower-energy states numerically from the mean-field equations based on the complex Ginzburg-Landau equation (GLE) written for the condensate wave function ψ [49,50]. In Ref. [10] we established the set of parameters of the mean-field model of the polariton condensate that reproduces the experimental data across the full range of distances. In what follows, we use the same dimensionless model

$$i\frac{\partial\psi}{\partial t} = -(1 - i\eta\mathcal{R})\nabla^2\psi + |\psi|^2\psi + g\mathcal{R}\psi + i(\mathcal{R} - \gamma)\psi, \tag{3}$$

$$\frac{\partial\mathcal{R}}{\partial t} = -(1 + b|\psi|^2)\mathcal{R} + P(\mathbf{r}), \tag{4}$$

and the same set of the parameters and nondimensionalization as in Ref. [10]. Here, $\mathcal{R}$ is the dimensionless density profile of the exciton reservoir, g corresponds to the blueshift due to interactions with noncondensed particles, γ represents the decay rates of condensed polaritons, b is proportional to the ratio of the rate at which the exciton reservoir feeds the condensate and the strength of effective polariton-polariton interaction, and η is the energy relaxation coefficient specifying the rate at which gain decreases with increasing energy. The

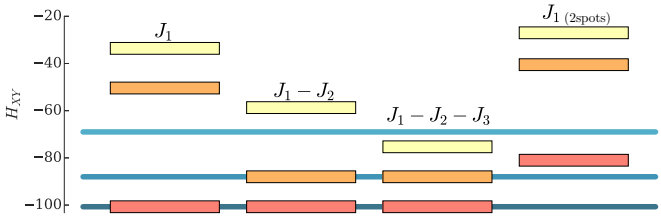

FIG. 3. The comparison of the lowest-energy levels of the four different XY models, depicted with rectangles, with the polariton particle mass residues found from the GLE, depicted with blue solid lines, for the hexagon with the lattice constant 11.5 μm. The first column shows energy levels in case of the XY model including nearest-neighbor interactions J_1, the second and the third columns include second-neighbor interactions J_1-J_2 and the second- and the third-neighbor interactions J_1-J_2-J_3, respectively. These three models are based on the coupling strengths that are found through the analysis of the hexagon of polariton condensates. The last column shows the energy states of the XY model with nearest-neighbor interactions $J_{1\ (2\ \text{spots})}$ based on the couplings obtained from the analysis of the two isolated polariton condensates.

nondimensionalization is chosen so that the unit length is 1 μm. For a hexagon side d between 8 and 16 μm, we find the stationary states by numerically integrating Eqs. (3) and (4) starting from a hundred randomly distributed fields $\psi(\mathbf{r}, t = 0) = \sum a_{\mathbf{k}} \exp(i\mathbf{k} \cdot \mathbf{r})$, where the phases of the complex amplitudes $a_{\mathbf{k}}$ are distributed uniformly on $[0, 2\pi]$ [51]. The corresponding particle mass residues are shown in Figs. 1(a) and 1(c) with solid circles, where the different colors correspond to various phase differences between the hexagon vertices. For the parameters and distances considered, the polariton ground state has always 0 [ferromagnetic (F)] or π [antiferromagnetic (AF)] phase differences. For a F ground state the first and the second excited states are always a single vortex with $\theta_{ij} = \pi/3$ and a spin wave with $\theta_{ijk} = \{\pi, 0, 0\}$, respectively, where j and k stand for the short notation of adjacent condensates $i+1$ and $i+2$, respectively. For an AF ground state, these are a double vortex with $\theta_{ij} = 2\pi/3$ and a spin wave with $\theta_{ijk} = \{0, \pi, \pi\}$, respectively.

We can accurately estimate the coupling strengths for each hexagon side d by solving the matrix equation $\mathbf{M} = \mathcal{B}\mathbf{J}$, where $\mathbf{M} = [\mathcal{M}_0, \mathcal{M}_1, \mathcal{M}_2]^T$, $\mathbf{J} = [J_1, J_2, J_3]^T$, and the matrix $\mathcal{B}$ has elements $b_{mj} = q_j \sum_{i=1}^{6} \cos\theta_{ii+j}^{m}$, $q_1 = q_2 = 1$, $q_3 = 1/2$. Here, the elements of $\mathbf{M}$ are the particle number residues for the ground, the first and the second excited states of the polariton graph, respectively, and m indexes the phases of the corresponding states. First, we neglect J_3 interactions (J_1-J_2 model) and calculate the ratios of $J_1/|J_1|$ and $J_2/|J_1|$, that are shown in Fig. 1(b) with blue and green circles, respectively. We use the obtained J_1 and J_2 for each d to minimize the XY Hamiltonian by running the gain-dissipative algorithm [52] on 1000 random initial conditions. The resulting energies of the ground state and the two lowest excited states are denoted by solid squares in Fig. 1(a) and show a good correspondence between the GLE and the XY model for the ground and the first excited states in terms of both the observed phase configurations and the

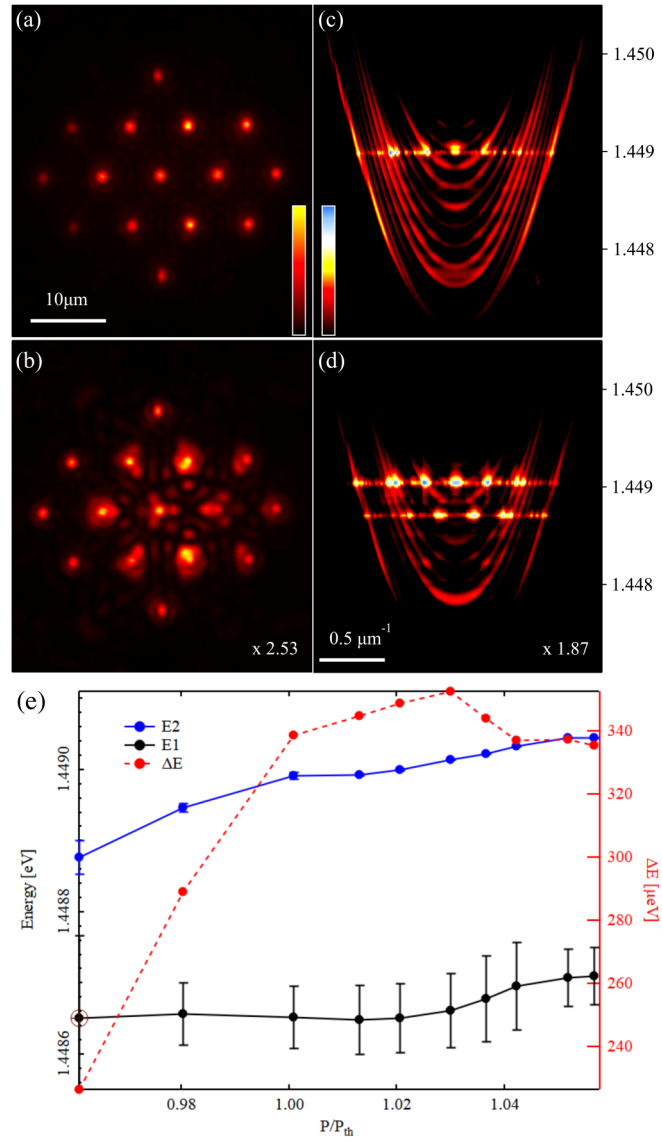

FIG. 4. (a), (b) Real space and (c), (d) energy dispersion of the false color plots for two densities of a triangular lattice of condensates. (a), (c) For $P = 1.01P_{\text{th}}$ the system is in a single stable configuration. (b), (d) For $P = 1.05P_{\text{th}}$ a second energy state emerges. The color scale in (c) and (d) is logarithmic while the dispersion replicas are due to imaging through the substrate. For an increased lattice size $d = 10$ μm, the dependence of the two lowest-energy levels and their difference (energy gap) on the pumping intensity above the condensation threshold is shown in (e).

energy values. The phase configurations for the second excited states are generally predicted correctly and the energies are in a fair agreement. Figures 1(c) and 1(d) show the results for the solution of the full matrix equation (the J_1-J_2-J_3 model), where a good agreement between all three states is illustrated. The six distinct phase configurations that were observed for different hexagon sides d in Figs. 1(a) and 1(c) are shown in Fig. 2 superimposed on the polariton densities.

We summarize the differences between the energies and phase configurations of states found by a polariton graph and those predicted by the direct minimization of the XY

Hamiltonian in Fig. 3 for a particular hexagon side d. On this figure the polariton particle mass residues (blue lines) are compared with the energy levels of the XY model (squares) taking into account various many-body interactions: nearest J_1, nearest and next-nearest J_1-J_2, all pairwise J_1-J_2-J_3, as well as nearest-neighbor interactions obtained from the GLE model for two pumping spots only. The phase configurations (shown by various colors) coincide in all cases. The agreement between excited states becomes better when the further couplings J_2 and J_3 beyond the nearest neighbors are introduced. The discrepancy between the energies of the ground states of the polariton particle mass residues and the XY model, based on the coupling strengths J_1 of two isolated pumping spots, is contributed to the density enhancement from the remaining spots that change the outflow velocity k_c and therefore the coupling strength.

Energy gap experiment. In order to experimentally elucidate the appearance of the gap as the system is pumped well above the threshold, we create a triangular lattice of 15 interacting polariton condensates and probe the energy state of the system. We excite the system nonresonantly with an ultranarrow linewidth continuous-wave coherent optical source spatially shaped into the desired lattice arrangement with the use of a phase spatial light modulator, while the phase pattern has been calculated with the use of an iterative Fourier-transform algorithm [53]. The spatially patterned light source is then projected on a high q-factor microcavity sample, that we have previously used to demonstrate polariton condensation [54], at a detuning of $\Delta = -2$ meV. We then image the real space and energy dispersion of the polariton emission in transmission. For an optical excitation density around threshold ($P_1 = 1.01P_{\text{th}}$) where all our excitation spots are above threshold [Fig. 4(a)] we observe as we expect a single energy state with a resolution-limited linewidth of $\Delta E_1 = 30 \pm 25$ μeV [Fig. 4(c)]. Increasing the polariton density by tuning the optical density to $P_2 = 1.05P_{\text{th}}$, we observe the emergence of an additional interferometric pattern in the condensate lattice [Fig. 4(b)]. The energy dispersion for this configuration reveals the emergence of a resolution-limited energy level at an energy difference of $\Delta E_{12} = 334 \pm 42$ μeV. Once one changes the lattice size, the nonzero energy gap could be observed even at the condensation threshold. In Fig. 4(e) the energy gap exhibits a nonlinear behavior with respect to the pumping intensity and does not close near P_{th}. Such a gapped system forms when the distance between the condensates is away from the center of a F or AF zone in Fig. 1 and represents an oscillatory state between the two lowest-energy levels, as was observed experimentally for a polariton dyad [55].

In conclusion, the "particle mass residues" of successive states in polariton graphs, that occur with increasing excitation density above the condensation threshold, could fairly approximate the XY Hamiltonian's energy spectrum. We confirm it by calculating phase configurations and spectra of polariton condensates for a range of hexagonal lattice sizes using a mean-field theory (GLE), which are found to be in a good agreement with the energy spectra derived from the XY model. The established correspondence between the driven-dissipative condensate system and the XY model paves the way for using such a platform for analog Hamiltonian simulations. We have experimentally implemented a triangular lattice of polariton condensates and have shown the emergence of a spectral gap as the pumping increases above the threshold. We have also found the regime in which the gapped state could be observed even at the condensation threshold. The spectral gap depends on the number of lattice sites, on how far above the threshold the pumping is, and what kind of coupling is established. The nonlinear behavior of the coupling strength as a function of pumping and the distance between the sites leads to the nonlinear dependence of the gap size on the gain. The further understanding of the influence of all these parameters on the gap size is a subject of our future theoretical and experimental work. The system is scalable and limited only by the size of the sample, which is typically a couple of square millimeters, and the distance between the condensates, which can be as small as 10 μm, so up to few thousand lattice sites can be realized in the present experimental conditions. With a resolution-limited energy level of 40 μeV we can expect to resolve the spectral gap for large systems.

N.G.B. acknowledges financial support from Huawei. K.P.K. acknowledges the financial support from Cambridge Trust and NPIF EPSRC Doctoral Grant No. EP/R512461/1.

[1] M. B. Hastings and T. Koma, Spectral gap and exponential decay of correlations, Commun. Math. Phys. **265**, 781 (2006).
[2] D. Aharonov, W. Van Dam, J. Kempe, Z. Landau, S. Lloyd, and O. Regev, Adiabatic quantum computation is equivalent to standard quantum computation, SIAM J. Comput. **37**, 166 (2007).
[3] E. Farhi, J. Goldstone, S. Gutmann, and M. Sipser, Quantum computation by adiabatic evolution, arXiv:quant-ph/0001106.
[4] F. D. M. Haldane, Nonlinear Field Theory of Large-Spin Heisenberg Antiferromagnets: Semiclassically Quantized Solitons of the One-Dimensional Easy-Axis Néel State, Phys. Rev. Lett. **50**, 1153 (1983).
[5] P. W. Anderson, Resonating valence bonds: A new kind of insulator? Mater. Res. Bull. **8**, 153 (1973).
[6] T. S. Cubitt, D. Perez-Garcia, and M. M. Wolf, Undecidability of the spectral gap, Nature (London) **528**, 207 (2015).
[7] I. M. Georgescu, S. Ashhab, and F. Nori, Quantum simulation, Rev. Mod. Phys. **86**, 153 (2014).
[8] S. Utsunomiya, K. Takata and Y. Yamamoto, Mapping of Ising models onto injection-locked laser systems, Opt. Express **19**, 18091 (2011).
[9] A. Marandi, Z. Wang, K. Takata, R. L. Byer, and Y. Yamamoto, Network of time-multiplexed optical parametric oscillators as a coherent Ising machine, Nat. Photonics **8**, 937 (2014).
[10] N. G. Berloff, K. Kalinin, M. Silva, W. Langbein, and P. G. Lagoudakis, Realizing the classical XY Hamiltonian in polariton simulators, Nat. Mater. **16**, 1120 (2017).

[11] M. Nixon, E. Ronen, A. A. Friesem, and N. Davidson, Observing Geometric Frustration with Thousands of Coupled Lasers, Phys. Rev. Lett. **110**, 184102 (2013).

[12] D. V. Vaidya, Y. Guo, Ronen M. Kroeze, K. E. Ballantine, A. J. Kollr, J. Keeling, and B. L. Lev, Tunable-Range, Photon-Mediated Atomic Interactions in Multimode Cavity QED, Phys. Rev. X **8**, 011002 (2018).

[13] D. Dung, C. Kurtscheid, T. Damm, J. Schmitt, F. Vewinger, M. Weitz, and J. Klaers, Variable potentials for thermalized light and coupled condensates, Nat. Photonics **11**, 565 (2017).

[14] M. Lewenstein, A. Sanpera, V. Ahufinger, B. Damski, A. Sen, and U. Sen, Ultracold atomic gases in optical lattices: Mimicking condensed matter physics and beyond, Adv. Phys. **56**, 243 (2007).

[15] M. Saffman, T. G. Walker, and K. Molmer, Quantum information with Rydberg atoms, Rev. Mod. Phys. **82**, 2313 (2010).

[16] J. Simon, W. S. Bakr, R. Ma, M. E. Tai, Ph. M. Preiss, and M. Greiner, Quantum simulation of antiferromagnetic spin chains in an optical lattice, Nature (London) **472**, 307 (2011).

[17] T. Esslinger, Fermi-Hubbard physics with atoms in an optical lattice, Annu. Rev. Condens. Matter Phys. **1**, 129 (2010).

[18] K. Kim, M.-S. Chang, S. Korenblit, R. Islam, E. E. Edwards, J. K. Freericks, G.-D. Lin, L.-M. Duan, and C. Monroe, Quantum simulation of frustrated Ising spins with trapped ions, Nature (London) **465**, 590 (2010).

[19] B. P. Lanyon, C. Hempel, D. Nigg, M. Muller, R. Gerritsma, F. Zahringer, P. Schindler, J. T. Barreiro, M. Rambach, G. Kirchmair, and M. Hennrich, Universal digital quantum simulation with trapped ions, Science **334**, 57 (2011).

[20] T. E. Northup and R. Blatt, Quantum information transfer using photons, Nat. Photonics **8**, 356 (2014).

[21] A. D. Corcoles, E. Magesan, S. J. Srinivasan, A. W. Cross, M. Steffen, J. M. Gambetta, and J. M. Chow, Demonstration of a quantum error detection code using a square lattice of four superconducting qubits, Nat. Commun. **6**, 6979 (2015).

[22] G. D. Cuevas and T. S. Cubitt, Simple universal models capture all classical spin physics, Science **351**, 1180 (2016).

[23] C. Weisbuch, M. Nishioka, A. Ishikawa, and Y. Arakawa, Observation of the Coupled Exciton-Photon Mode Splitting in a Semiconductor Quantum Microcavity, Phys. Rev. Lett. **69**, 3314 (1992).

[24] J. Kasprzak, M. Richard, S. Kundermann, A. Baas, P. Jeambrun, J. M. J. Keeling, F. M. Marchetti, M. H. Szymańska, R. André, J. L. Staehli, and V. Savona, Bose-Einstein condensation of exciton polaritons, Nature (London) **443**, 409 (2006).

[25] J. Keeling and N. G. Berloff, Exciton-polariton condensation, Contemp. Phys. **52**, 131 (2011).

[26] I. Carusotto and C. Ciuti, Quantum fluids of light, Rev. Mod. Phys. **85**, 299 (2013).

[27] J. Keeling and N. G. Berloff, Controllable half-vortex lattices in an incoherently pumped polariton condensate, arXiv:1102.5302.

[28] G. Tosi, G. Christmann, N. G. Berloff, P. Tsotsis, T. Gao, Z. Hatzopoulos, P. G. Savvidis, and J. J. Baumberg, Sculpting oscillators with light within a nonlinear quantum fluid, Nat. Phys. **8**, 190 (2012).

[29] G. Tosi, G. Christmann, N. G. Berloff, P. Tsotsis, T. Gao, Z. Hatzopoulos, P. G. Savvidis, and J. J. Baumberg, Geometrically locked vortex lattices in semiconductor quantum fluids, Nat. Commun. **3**, 1243 (2013).

[30] H. Ohadi, R. L. Gregory, T. Freegarde, Y. G. Rubo, A. V. Kavokin, N. G. Berloff, and P. G. Lagoudakis, Nontrivial Phase Coupling in Polariton Multiplets, Phys. Rev. X **6**, 031032 (2016).

[31] K. P. Kalinin and N. G. Berloff, Polaritonic network as a paradigm for dynamics of coupled oscillators, Phys. Rev. B **100**, 245306 (2019).

[32] K. P. Kalinin and N. G. Berloff, Simulating Ising and Potts Models and External Fields with Non-Equilibrium Condensates, Phys. Rev. Lett. **121**, 235302 (2018).

[33] K. P. Kalinin, A. Amo, J. Bloch, and N. G. Berloff, Polaritonic XY-Ising machine, Nanophotonics **9**, 4127 (2020).

[34] H. Deng, G. Weihs, C. Santori, J. Bloch, and Y. Yamamoto, Condensation of semiconductor microcavity exciton polaritons, Science **298**, 199 (2002).

[35] T. E. Lee and C. K. Chan, Heralded Magnetism in Non-Hermitian Atomic Systems, Phys. Rev. X **4**, 041001 (2014).

[36] W. D. Heiss, The physics of exceptional points, J. Phys. A **45**, 444016 (2012).

[37] Y. Kominis, V. Kovanis, and T. Bountis, Spectral signatures of exceptional points and bifurcations in the fundamental active photonic dimer, Phys. Rev. A **96**, 053837 (2017).

[38] J. Wordsworth and P. Ashwin, Spatiotemporal coding of inputs for a system of globally coupled phase oscillators, Phys. Rev. E **78**, 066203 (2008).

[39] F. S. Neves and M. Timme, Computation by Switching in Complex Networks of States, Phys. Rev. Lett. **109**, 018701 (2012).

[40] N. Stroev and N. G. Berloff, Discrete polynomial optimization with coherent networks of condensates and complex coupling switching, arXiv:1910.00842.

[41] P. Hauke, T. Roscilde, V. Murg, J. I. Cirac, and R. Schmied, Modified spin-wave theory with ordering vector optimization: frustrated bosons on the spatially anisotropic triangular lattice, New J. Phys. **12**, 053036 (2010).

[42] F. Figueirido, A. Karlhede, S. Kivelson, S. Sondhi, M. Rocek, and D. S. Rokhsar, Exact diagonalization of finite frustrated spin-1/2 Heisenberg models, Phys. Rev. B **41**, 4619 (1990).

[43] N. Read and S. Sachdev, Large-N Expansion for Frustrated Quantum Antiferromagnets, Phys. Rev. Lett. **66**, 1773 (1991).

[44] R. Darradi, O. Derzhko, R. Zinke, J. Schulenburg, S. E. Kruger, and J. Richter, Ground state phases of the spin-1/2 J_1–J_2 Heisenberg antiferromagnet on the square lattice: A high-order coupled cluster treatment, Phys. Rev. B **78**, 214415 (2008).

[45] C. N. Varney, K. Sun, V. Galitski, and M. Rigol, Kaleidoscope of Exotic Quantum Phases in a Frustrated XY Model, Phys. Rev. Lett. **107**, 077201 (2011).

[46] Zh. Zhu, D. A. Huse, and S. R. White, Unexpected Z-Direction Ising Antiferromagnetic Order in a Frustrated spin-1/2 J_1 – J_2 XY Model on the Honeycomb Lattice, Phys. Rev. Lett. **111**, 257201 (2013).

[47] R. F. Bishop, P. H. Y. Li, D. J. J. Farnell, and C. E. Campbell, The frustrated Heisenberg antiferromagnet on the honeycomb lattice: J_1–J_2 model, J. Phys.: Condens. Matter **24**, 236002 (2012).

[48] H. Mosadeq, F. Shahbazi, and S. A. Jafari, Plaquette valence bond ordering in a J_1-J_2 Heisenberg antiferromagnet on a honeycomb lattice, J. Phys.: Condens. Matter **23**, 226006 (2011).

[49] M. Wouters and I. Carusotto, Excitations in a Nonequilibrium Bose-Einstein Condensate of Exciton Polaritons, Phys. Rev. Lett. **99**, 140402 (2007).

[50] J. Keeling and N. G. Berloff, Spontaneous Rotating Vortex Lattices in a Pumped Decaying Condensate, Phys. Rev. Lett. **100**, 250401 (2008).

[51] N. G. Berloff and B. V. Svistunov, Scenario of strongly nonequilibrated Bose-Einstein condensation, Phys. Rev. A **66**, 013603 (2002).

[52] K. P. Kalinin and N. G. Berloff, Global optimization of spin Hamiltonians with gain-dissipative systems, Sci. Rep. **8**, 17791 (2018).

[53] M. Pasienski and B. DeMarco, A high-accuracy algorithm for designing arbitrary holographic atom traps, Opt. Express **16**, 2176 (2008).

[54] P. Cilibrizzi, A. Askitopoulos, M. Silva, F. Bastiman, E. Clarke, J. M. Zajac, W. Langbein, and P. G. Lagoudakis, Polariton condensation in a strain-compensated planar microcavity with InGaAs quantum wells, Appl. Phys. Lett. **105**, 191118 (2014).

[55] J. D. Topfer, H. Sigurdsson, L. Pickup, and P. G. Lagoudakis, Time-delay polaritonics, Commun. Phys. **3**, 2 (2020).